Iron Vacancy Tunable Superconductor-Insulator Transition in $FeSe/SrTiO_3$ Monolayer

Cheng-Long Xue,[1] Li-Guo Dou,[1] Yong-Jie Xu,[1] Qian-Qian Yuan,[1] Qi-Yuan Li,[1] Zhen-Yu Jia,[1] Zishuang Li,[1] Ronghua Liu,[1,2,3] and Shao-Chun Li[1,2,3,4,*]

[1]*National Laboratory of Solid State Microstructures, School of Physics, Nanjing University, Nanjing 210093, China*
[2]*Collaborative Innovation Center of Advanced Microstructures, Nanjing University, Nanjing 210093, China*
[3]*Jiangsu Provincial Key Laboratory for Nanotechnology, Nanjing University, Nanjing 210093, China*
[4]*Hefei National Laboratory, Hefei 230088, China*

(Received 5 April 2023; revised 15 November 2023; accepted 21 November 2023; published 20 December 2023)

The Fe_4Se_5 with a $\sqrt{5} \times \sqrt{5}$ Fe vacancy order is suggested to be a Mott insulator and the parent state of bulk FeSe superconductor. The iron vacancy ordered state has been considered as a Mott insulator and the parent compound of bulk FeSe-based superconductors. However, for the superconducting $FeSe/SrTiO_3$ monolayer (FeSe/STO) with an interface-enhanced high transition temperature (T_c), the electronic evolution from its Fe vacancy ordered parent phase to the superconducting state, has not been explored due to the challenge to realize an Fe vacancy order in the FeSe/STO monolayer, even though important to the understanding of superconductivity mechanism. In this study, we developed a new method to generate Fe vacancies within the FeSe/STO monolayer in a tunable fashion, with the assistance of atomic hydrogen. As a consequence, an insulating $\sqrt{5} \times \sqrt{5}$ Fe vacancy ordered monolayer is realized as the parent state. By using scanning tunneling microscopy and scanning tunneling spectroscopy, the spectral evolution from superconductivity to insulator is fully characterized. Surprisingly, a prominent spectral weight transfer occurs, thus implying a strong electron correlation effect. Moreover, the Fe vacancy induced insulating gap exhibits no Mott gap-like features. This work provides new insights in understanding the high-T_c superconductivity in FeSe/STO monolayer.

DOI: 10.1103/PhysRevLett.131.256002

Unconventional superconductors have attracted great attention in condensed matter physics because of the high transition temperature (T_c) and rich interplay between magnetism, nematicity, and topology, etc. [1–5]. Superconductivity can be realized via doping the parent compounds [6]. The parent compounds of cuprates are usually antiferromagnetic Mott insulators, while in iron pnictides-based superconductors, the parent compounds mostly exhibit a metallic behavior with an antiferromagnetic order [1,7–9]. Bulk FeSe superconductor hosts the simplest chemical and crystal structure with a T_c of 8 K [10], and resides evidently in the vicinity of iron-vacancy ordered insulating phases. The Fe_4Se_5 with a $\sqrt{5} \times \sqrt{5}$ Fe vacancy order was suggested to be a Mott insulating parent compound, which undergoes a superconductivity transition after annealing to annihilate or melt the Fe vacancy [11,12]. Both of the $\sqrt{5} \times \sqrt{5}$ ordered bulk and multilayered FeSe were reported to host an antiferromagnetic order [11–14]. Similarly, the $\sqrt{5} \times \sqrt{5}$ Fe vacancy ordered $K_2Fe_4Se_5$ was also suggested to be the Mott insulating parent compound for $K_xFe_{2-y}Se_2$ superconductor [15–17].

The epitaxial $FeSe/SrTiO_3$ (FeSe/STO) monolayer hosts an interface-enhanced superconductivity [18–33]. Even though still debated, it is basically established that the high-T_c in FeSe/STO monolayer originates from a cooperative effect of interfacial charge transfer and electron-phonon coupling [19,21,30]. However, it still remains elusive whether the $\sqrt{5} \times \sqrt{5}$ Fe vacancy ordered monolayer can be experimentally realized as the parent compound [12]. It has been believed that the $\sqrt{5} \times \sqrt{5}$ Fe vacancy ordered state cannot form in the FeSe/STO monolayer, presumably because of the strong interfacial binding effect. It is noteworthy that to investigate its parent phase and the doping induced spectral evolution is significantly important to the in-depth understanding of the superconductivity mechanism in the FeSe/STO monolayer.

In this Letter, we developed a hydrogen-assisted method to precisely produce Fe vacancies in the FeSe/STO monolayer, as illustrated in Fig. 1(a). Through this method, Fe vacancies were gradually introduced into the superconducting FeSe/STO monolayer, finally resulting in an insulating Fe vacancy order with a $\sqrt{5} \times \sqrt{5}$ period. This superconductor-insulator transition is the reverse process of electron doping to the Fe vacancy ordered parent compound. By using scanning tunneling microscopy (STM) and scanning tunneling spectroscopy (STS), we recorded the detailed spectral evolution during the whole transition, and revealed a prominent spectral weight transfer instead of a Fermi level shift as expected for the hole doping, which may imply a strong electron correlation effect. We also

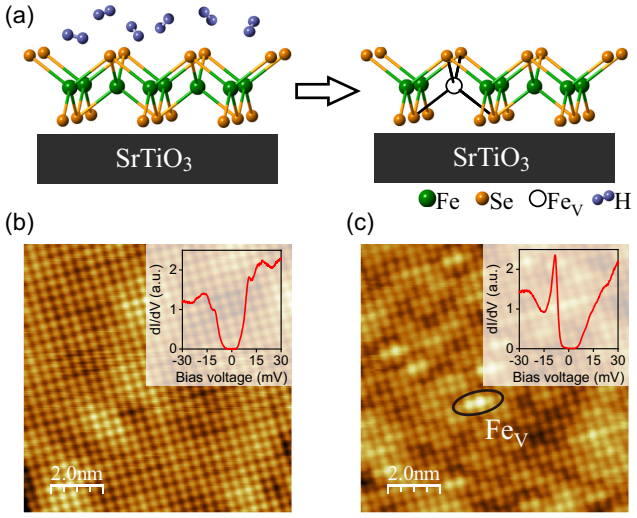

FIG. 1. Hydrogen exposure induced Fe vacancies in the superconducting FeSe/STO monolayer. (a) Schematic illustration of generating Fe vacancy via hydrogen exposure. (b),(c) Atomically resolved topographic images (10×10 nm^2) of the superconducting FeSe/STO monolayer before and after exposure to a small amount of atomic hydrogen. $U = +400$ mV, $I_t = 1$ nA for (b) and $U = +100$ mV, $I_t = 1$ nA for (c). The black elliptical in (c) outlines the Fe vacancy. Insets: dI/dV spectra taken on the clean surface (b) and the Fe vacancy (c).

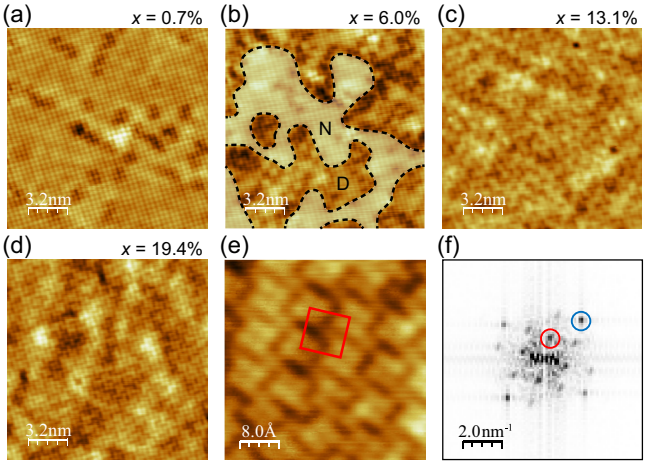

FIG. 2. Topographic evolution of the FeSe/STO monolayer as a function of hydrogen exposure. (a) Topographic images (16×16 nm^2) with randomly distributed Fe vacancies. $U = +0.2$ V, $I_t = 1$ nA. (b) Topographic images (16×16 nm^2) of the two distinguishable regions with the different populations of Fe vacancy. $U = +1$ V, $I_t = 2$ nA. N region has a low density of Fe vacancies, and D region a high density of Fe vacancies. (c) Topographic images (16×16 nm^2) with ordered Fe vacancies. $U = +2$ V, $I_t = 3$ nA. (d) Topographic images (16×16 nm^2) with long-range coherent Fe vacancy order upon the gentle low temperature annealing. $U = +2$ V, $I_t = 2$ nA. (e) Atomically resolved STM topographic image (4×4 nm^2) of the $\sqrt{5} \times \sqrt{5}$ order. $U = +2$ V and $I_t = 1$ nA. The red square marks the unit cell of the Fe vacancies order. (f) Fast Fourier transform of (e). The red and blue circles mark the $\sqrt{5} \times \sqrt{5}$ order and the lattice Bragg point, respectively.

found that the insulating gap in the Fe vacancy ordered monolayer exhibits no Mott gaplike features. These observations provide insights into understanding the high-T_c superconductivity in the FeSe/STO monolayer.

The as-grown FeSe/STO monolayer exhibits no superconductivity transition, and the following postannealing can establish a superconductivity transition with an energy gap of ~16 mV (see Supplemental Material, Fig. S1 [34]). The atomically resolved topographic image, Fig. 1(b), reveals a perfectly ordered Se-terminated (001) lattice, and the dI/dV spectrum, the inset to Fig. 1(b), reveals a typical superconducting gap with double coherence peaks at $\sim \pm 9$ mV and $\sim \pm 16$ mV. Figure 1(c) shows the high-resolution topographic image of FeSe/STO monolayer after *in situ* exposure to a small amount of atomic hydrogen of 2.4 L (Langmuir, 1 L $= 1.0 \times 10^{-6}$ Torrs). Surprisingly, some extra dumbbell-like species start to appear, as shown in Fig. 1(c). The dI/dV spectrum taken on top of these species, as plotted in the inset to Fig. 1(c), shows a peak at ~ -8.3 mV near the lower edge of the superconducting gap, a characteristic of Fe vacancy [35–37]. These H exposure-induced species can be attributed to the Fe vacancies. During exposure to H, the lattice Fe atoms are possibly facilitated to diffuse once bonded to H atom, and thus a Fe vacancy is formed in the FeSe lattice.

Superior to the widely adopted postannealing method to tune superconductivity, the H-facilitated process to generate Fe vacancy occurs only at room temperature, and the population of Fe vacancy is the only variable. We adopted this method to precisely control the population of Fe vacancy. For convenience, we use x to denote the Fe vacancy level in FeSe/STO monolayer, representing the average number of Fe vacancies per 1×1 unit cell of FeSe. Figure 2 shows a series of STM images after various amount of H exposure at room temperature (see also Supplemental Material, Figs. S2–S4 [34]). As the exposure time is extended, the population of Fe vacancies monotonously increases, see Figs. 2(a)–2(f) and Supplemental Material, Figs. S2–S4 [34]. Initially, as x is small [see Fig. 2(a)], the Fe vacancies are randomly distributed within the FeSe/STO monolayer. As x increases, for instance to ~6.0% in Fig. 2(b), the surface of FeSe/STO monolayer can be divided into two different regions. In addition to the normal area with a relatively low density of Fe vacancies (namely N regions), small patches with a locally high density of Fe vacancies (namely D regions) start to appear, as shown as in Fig. 2(b) and Supplemental Material, Fig. S3 [34]. As x further increases, the D regions with disordered Fe vacancies grow in size at the expense of the N regions, until the whole surface is completely covered by the locally ordered Fe vacancies, as shown in Fig. 2(c) (detailed evolution is shown in Supplemental Material, Figs. S3 and S4 [34]). As shown in Fig. 2(d), a gentle low

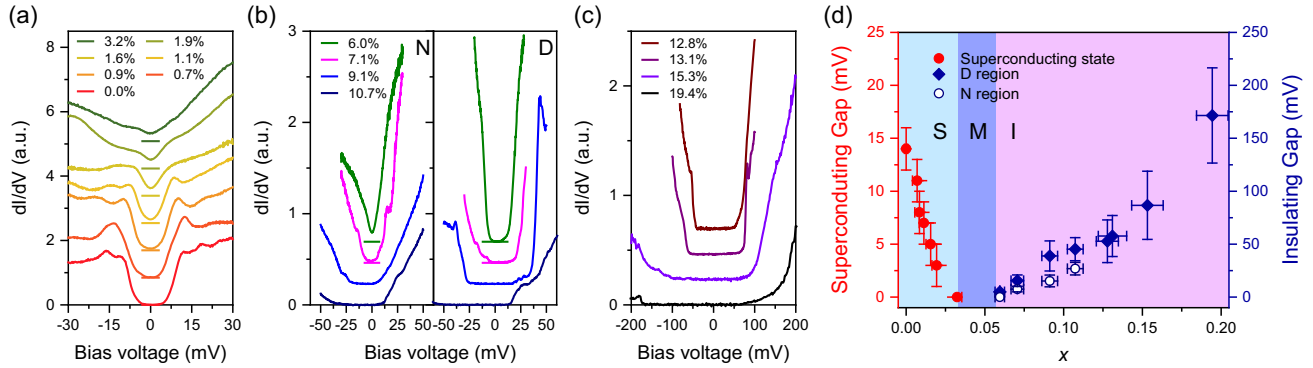

FIG. 3. Spectral evolution upon hydrogen exposure and phase diagram of the FeSe/STO monolayer. (a)–(c) dI/dV spectra evolution as a function of the Fe vacancy level. The spectra in (a)–(c) are uniformly shifted in the vertical direction for clarity. (d) Electronic phase diagram of the FeSe/STO monolayer as a function of the Fe vacancy level (x). Error bars are estimated from the standard deviation of the gap size measured at various locations. The superconductor (S), metal (M), and insulator (I) regions are specified with different colors, respectively.

temperature annealing to ~250 °C can greatly enhance the long-range coherence of the $\sqrt{5} \times \sqrt{5}$ order.

Along with the formation of Fe vacancies in the FeSe/STO monolayer, small second-layer islands of 1×1 order and ~0.56 nm high simultaneously appear as well, as shown in Supplemental Material, Figs. S2–S5 [34]. These islands are in fact the second layer FeSe formed by the kicked out Fe atoms from the first layer when Fe vacancies are formed. The Se atoms required to form the second layer FeSe may come from the excess Se layer at the FeSe/STO interface [28,38,39].

To further elucidate the impact of the Fe vacancies on superconductivity, we performed the STS measurements, as shown in Fig. 3(a) (more data can be found in Supplemental Material, Fig. S2 [34]). As the Fe vacancy level x increases, the FeSe/STO monolayer first exhibits a decreasing superconducting gap until closed at $x = \sim 3.2\%$. The superconductivity is then suppressed and the FeSe monolayer becomes a metal. In the following, the FeSe/STO monolayer undergoes a metal-insulator transition, exhibiting a growing insulating gap until the $\sqrt{5} \times \sqrt{5}$ Fe vacancy order is formed over the whole surface, see Figs. 3(b) and 3(c). It is noteworthy that the insulating gap measured in D regions (with a high density of Fe vacancy) is always larger than that in N region (with a low density of Fe vacancy), possibly due to the spatially inhomogeneous effect of Fe vacancy. As plotted in Fig. 3(d), an electronic phase diagram of the superconducting and insulating gaps versus Fe vacancy level (x) is established to illustrate the electronic evolution during the superconductor-metal-insulator transition.

Surprisingly, we found that the presence of even a small amount of disordered Fe vacancy can kill the superconductivity in FeSe/STO monolayer, possibly owing to an increased Coulomb repulsion that overpowers the attractive interaction responsible for Cooper pair formation [40]. This observation is consistent with some previous studies [36,41], but in contrast with the conclusion of some other studies that Fe vacancies may enhance the superconductivity [42–44]. The observation that the Fe vacancy $\sqrt{5} \times \sqrt{5}$ ordered monolayer hosts an insulating gap is in agreement with the previous studies for the bulk counterpart [11,12,15–17].

Next, we focus on the spectral weight evolution during the superconductor-metal-insulator transition. In Fig. 4(a) is plotted the series of large-scale STS spectrum with various Fe vacancy levels. For the STS spectrum taken on the superconducting FeSe/STO monolayer without a H exposure, two characteristics can be distinctly identified, i.e., the rather low and nearly flat differential conductance between ~ -65 mV to ~75 mV and the bumplike feature at ~ -250 mV as marked by the black triangle. The bump feature is possibly attributed to the Fe $3dz^2$ bands, according to the previous ARPES studies [45]. On the other hand, the bosonic mode-induced replica band is also located near this bump region [21,30,33]. Even though the two characteristics are spatially uniform for the superconducting FeSe/STO monolayer (see Supplemental Material, Fig. S6 [34]), they exhibit prominent spectral evolution during the superconductor-metal-insulator transition. Upon H exposure, the low differential conductance starts to increase gradually from both the band edges, as shown in Fig. 4(a). Meanwhile the bump intensity starts to decrease, and becomes spatially inhomogeneous as well. For example, within N and D regions, the intensity of the bump in D region is systematically lower than in N regions, as shown in Fig. 4(b). In the insulating state of $\sqrt{5} \times \sqrt{5}$ order, both the bump and low-intensity flat bottom completely disappear. We emphasize that a similar spectral weight transfer simultaneously occurs at the positive bias region as well. As shown in Fig. 4(b), the dI/dV intensity at $\sim +200$ mV is clearly decreased. The spectral difference, as obtained by subtracting a typical spectra in N region from one in D region, is plotted in Fig. 4(c), in order

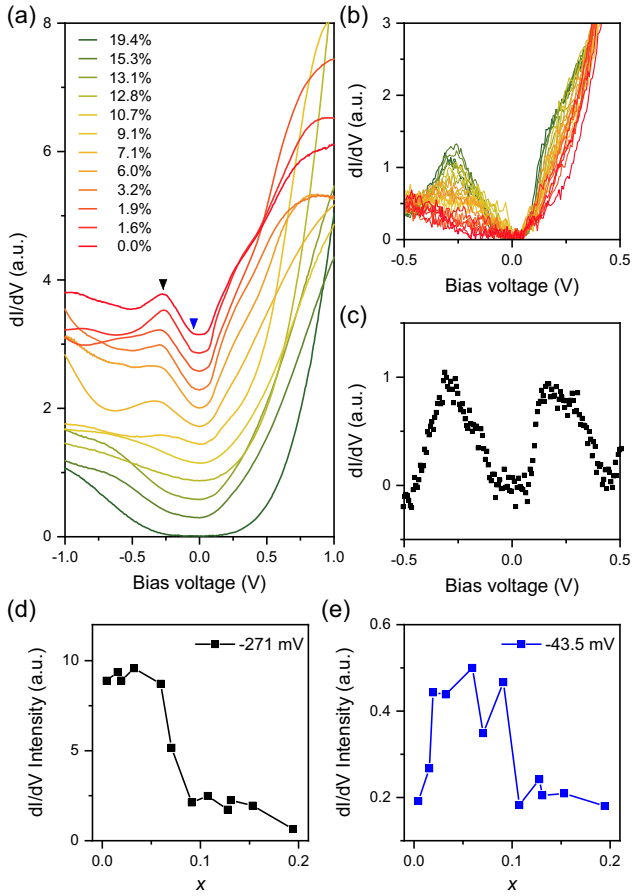

FIG. 4. Spectral weight evolution of the FeSe/STO monolayer during the superconductor-metal-insulator transition. (a) dI/dV spectra collected as a function of the Fe vacancy level. Each dI/dV spectra is averaged from multiple spectra taken at different locations of the same Fe vacancy level. The spectra are uniformly shifted in the vertical direction for clarity. (b) Series of dI/dV spectra taken from the region of low Fe vacancy level (N) to high Fe vacancy level (D). (c) Spectral difference obtained by subtracting a spectrum in N region from that in D region. (d), (e) dI/dV intensities of the bump at ~ -250 mV and the flat bottom at ~ -40 mV extracted from the positions as marked by the black and blue triangles in (a), respectively.

to neglect the influence of high spectral background at the positive bias voltage region. In Fig. 4(c), two symmetric bumps centered on the Fermi energy are clearly identified. It is thus indicated that the spectral weight evolution occurs symmetrically along Fermi energy at both negative and positive bias voltages. In the following, quantitative analysis is mainly made on the two characteristics. In Figs. 4(d) and 4(e) are plotted the average dI/dV intensities of the bump at ~ -250 mV and the flat bottom at ~ -40 mV, respectively. If comparing Fig. 3 to Fig. 4, one can tell that such spectral evolutions closely correlate with the superconductor-metal-insulator transition. It is noteworthy that this spectral weight evolution is beyond the influence of the single Fe vacancy, since a single Fe vacancy can only influence the spectral weight change within the FeSe unit cell. (The influence of the single iron vacancy is shown in Supplemental Material, Fig. S7 [34]).

The Fe vacancy ordered phase ($\sqrt{5} \times \sqrt{5}$) has been considered as a Mott insulator and the parent compound of bulk FeSe-based superconductors. The superconductivity transition can emerge through disordering the Fe vacancy order [11,12,15–17]. Analogous to its bulk counterpart, we realized the insulating $\sqrt{5} \times \sqrt{5}$ Fe vacancy order in FeSe/STO monolayer, and the superconductor-insulator transition via finely tuning the disordered and ordered Fe vacancies. The superconducting quantum interference device (SQUID) measurements suggested an antiferromagnetic behavior in the Fe vacancy ordered monolayer (Supplemental Material, Fig. S8 [34]).Even though the size of the insulating gap grows with the increasing Fe vacancies, the characteristic features of a Mott gap, such as lower and upper Hubbard bands that usually behave as the spectral peaks in dI/dV spectrum, are not experimentally identifiable. Moreover, the Fe vacancy level dependence of the insulating gap is also inconsistent with a typical Mott gap model. It thus points to a different scenario instead of doping a Mott insulator, regarding to the superconductivity in FeSe/STO monolayer.

To form a Fe vacancy in the FeSe/STO monolayer usually gives rise to an effective hole doping, and the Fermi level is expected to shift downward assuming a rigid band model. However, there exists no prominent Fermi energy shift during the superconductor-metal-insulator transition. Taking the bumplike feature as a reference, it is always located at ~ -250 mV until completely suppressed. Instead, the prominent spectral weight transfer implies that the rigid doping effect is negligible, and a strong electron correlation may play a dominant role [46]. A recent study reported that the $3d_{xz}/d_{yz}$ orbitals are primarily responsible for the electron pairing FeSe/STO monolayer [47]. Our observation that the superconductivity is promoted while the intensity of the bump is enhanced, which possibly suggests that the $3dz^2$ orbitals are participative for the pairing in FeSe/STO monolayer as well. If considering the symmetric spectral weight evolution along Fermi energy that is suppressed during the superconductor-metal-insulator transition, the bump feature is more likely to be originated from a bosonic mode instead of the dz^2 orbital. The energy of the bump feature is indeed very close to that of the replica band as reported in previous ARPES studies [21,30,33], thus implying a possible nature originating from the interfacial phonon coupling. Moreover, even though lack of direct evidence, the interfacial excess Se atoms, if existent [28,38], may act as the atom source for the formation of second layer FeSe, and thus play a role in tuning the interfacial phonon coupling, as manifested by the suppression of the bump feature. Our observation suggests that the uniform and stable bumplike feature in superconducting FeSe/STO monolayer may be a signature

of the interfacial electron-bosonic coupling that enhances superconductivity.

In summary, we have realized the superconductor-insulator transition in the FeSe/STO monolayer, through atomic hydrogen assisted introduction of disordered/ordered Fe vacancy. A spectral weight transfer, instead of a doping-induced Fermi energy shift, prominently occurs during the transition, and meanwhile no Mott-like features are identified in the Fe vacancy ordered parent state. Our study points to a different scenario instead of simply doping a Mott insulator.

This work was financially supported by the National Key Research and Development Program of China (Grant No. 2021YFA1400403), the National Natural Science Foundation of China (Grants No. 12374183, No. 92165205, No. 12074178, No. 11790311, No. 11774149) and Innovation Program for Quantum Science and Technology (Grant No. 2021ZD0302800).

C-L. X. and L-G. D. contributed equally to this work.

*scli@nju.edu.cn

[1] G. R. Stewart, Rev. Mod. Phys. **83**, 1589 (2011).
[2] M. K. Wu, P. M. Wu, Y. C. Wen, M. J. Wang, P. H. Lin, W. C. Lee, T. K. Chen, and C. C. Chang, J. Phys. D **48**, 323001 (2015).
[3] A. I. Coldea and M. D. Watson, Annu. Rev. Condens. Matter Phys. **9**, 125 (2018).
[4] A. Kreisel, P. J. Hirschfeld, and B. M. Andersen, Symmetry **12**, 1402 (2020).
[5] T. Shibauchi, T. Hanaguri, and Y. Matsuda, J. Phys. Soc. Jpn. **89**, 102002 (2020).
[6] P. A. Lee, N. Nagaosa, and X.-G. Wen, Rev. Mod. Phys. **78**, 17 (2006).
[7] W. Q. Chen, K. Y. Yang, Y. Zhou, and F. C. Zhang, Phys. Rev. Lett. **102**, 047006 (2009).
[8] M. M. Qazilbash, J. J. Hamlin, R. E. Baumbach, L. Zhang, D. J. Singh, M. B. Maple, and D. N. Basov, Nat. Phys. **5**, 647 (2009).
[9] Z. P. Yin, K. Haule, and G. Kotliar, Nat. Mater. **10**, 932 (2011).
[10] F. C. Hsu, J. Y. Luo, K. W. Yeh, T. K. Chen, T. W. Huang, P. M. Wu, Y. C. Lee, Y. L. Huang, Y. Y. Chu, D. C. Yan, and M. K. Wu, Proc. Natl. Acad. Sci. U.S.A. **105**, 14262 (2008).
[11] T. K. Chen, C. C. Chang, H. H. Chang, A. H. Fang, C. H. Wang, W. H. Chao, C. M. Tseng, Y. C. Lee, Y. R. Wu, M. H. Wen, H. Y. Tang, F. R. Chen, M. J. Wang, M. K. Wu, and D. V. Dyck, Proc. Natl. Acad. Sci. U.S.A. **111**, 63 (2014).
[12] K. Y. Yeh, Y. R. Chen, T. S. Lo, P. M. Wu, M. J. Wang, K. S. Chang-Liao, and M. K. Wu, Front. Phys. **8**, 567054 (2020).
[13] M. Gao, X. Kong, X.-W. Yan, Z.-Y. Lu, and T. Xiang, Phys. Rev. B **95**, 174523 (2017).
[14] W. Zhang, Z.-M. Zhang, J.-H. Nie, B.-C. Gong, M. Cai, K. Liu, Z.-Y. Lu, and Y.-S. Fu, Adv. Mater. **35**, 2209931 (2023).
[15] W. Bao, Q.-Z. Huang, G.-F. Chen, D.-M. Wang, J.-B. He, and Y.-M. Qiu, Chin. Phys. Lett. **28**, 086104 (2011).
[16] C.-H. Wang, T.-K. Chen, C.-C. Chang, C.-H. Hsu, Y.-C. Lee, M.-J. Wang, P. M. Wu, and M.-K. Wu, Europhys. Lett. **111**, 27004 (2015).
[17] C. H. Wang, C. C. Lee, G. T. Huang, J. Y. Yang, M. J. Wang, H. S. Sheu, J. J. Lee, and M. K. Wu, Proc. Natl. Acad. Sci. U.S.A. **116**, 1104 (2019).
[18] Q.-Y. Wang, Z. Li, W.-H. Zhang, Z.-C. Zhang, J.-S. Zhang, W. Li, H. Ding, Y.-B. Ou, P. Deng, K. Chang, J. Wen, C.-L. Song, K. He, J.-F. Jia, S.-H. Ji, Y.-Y. Wang, L.-L. Wang, X. Chen, X.-C. Ma, and Q.-K. Xue, Chin. Phys. Lett. **29**, 037402 (2012).
[19] D. Liu, W. Zhang, D. Mou, J. He, Y. B. Ou, Q. Y. Wang, Z. Li, L. Wang, L. Zhao, S. He, Y. Peng, X. Liu, C. Chen, L. Yu, G. Liu, X. Dong, J. Zhang, C. Chen, Z. Xu, J. Hu, X. Chen, X. Ma, Q. Xue, and X. J. Zhou, Nat. Commun. **3**, 931 (2012).
[20] S. Tan, Y. Zhang, M. Xia, Z. Ye, F. Chen, X. Xie, R. Peng, D. Xu, Q. Fan, H. Xu, J. Jiang, T. Zhang, X. Lai, T. Xiang, J. Hu, B. Xie, and D. Feng, Nat. Mater. **12**, 634 (2013).
[21] J. J. Lee, F. T. Schmitt, R. G. Moore, S. Johnston, Y. T. Cui, W. Li, M. Yi, Z. K. Liu, M. Hashimoto, Y. Zhang, D. H. Lu, T. P. Devereaux, D. H. Lee, and Z. X. Shen, Nature (London) **515**, 245 (2014).
[22] S. Coh, M. L. Cohen, and S. G. Louie, New J. Phys. **17**, 073027 (2015).
[23] J. F. Ge, Z. L. Liu, C. Liu, C. L. Gao, D. Qian, Q. K. Xue, Y. Liu, and J. F. Jia, Nat. Mater. **14**, 285 (2015).
[24] Y. Miyata, K. Nakayama, K. Sugawara, T. Sato, and T. Takahashi, Nat. Mater. **14**, 775 (2015).
[25] A. Linscheid, S. Maiti, Y. Wang, S. Johnston, and P. J. Hirschfeld, Phys. Rev. Lett. **117**, 077003 (2016).
[26] D. Huang and J. E. Hoffman, Annu. Rev. Condens. Matter Phys. **8**, 311 (2017).
[27] X. Shi, Z. Q. Han, X. L. Peng, P. Richard, T. Qian, X. X. Wu, M. W. Qiu, S. C. Wang, J. P. Hu, Y. J. Sun, and H. Ding, Nat. Commun. **8**, 14988 (2017).
[28] W. Zhao, M. Li, C. Z. Chang, J. Jiang, L. Wu, C. Liu, J. S. Moodera, Y. Zhu, and M. H. W. Chan, Sci. Adv. **4**, eaao2682 (2018).
[29] Z. Ge, C. Yan, H. Zhang, D. Agterberg, M. Weinert, and L. Li, Nano Lett. **19**, 2497 (2019).
[30] Q. Song, T. L. Yu, X. Lou, B. P. Xie, H. C. Xu, C. H. P. Wen, Q. Yao, S. Y. Zhang, X. T. Zhu, J. D. Guo, R. Peng, and D. L. Feng, Nat. Commun. **10**, 758 (2019).
[31] S. Zhang, T. Wei, J. Guan, Q. Zhu, W. Qin, W. Wang, J. Zhang, E. W. Plummer, X. Zhu, Z. Zhang, and J. Guo, Phys. Rev. Lett. **122**, 066802 (2019).
[32] B. D. Faeth, S. L. Yang, J. K. Kawasaki, J. N. Nelson, P. Mishra, C. T. Parzyck, C. Li, D. G. Schlom, and K. M. Shen, Phys. Rev. X **11**, 021054 (2021).
[33] C. Liu, R. P. Day, F. Li, R. L. Roemer, S. Zhdanovich, S. Gorovikov, T. M. Pedersen, J. Jiang, S. Lee, M. Schneider, D. Wong, P. Dosanjh, F. J. Walker, C. H. Ahn, G. Levy, A. Damascelli, G. A. Sawatzky, and K. Zou, Nat. Commun. **12**, 4573 (2021).
[34] See Supplemental Material at http://link.aps.org/supplemental/10.1103/PhysRevLett.131.256002 for details of experimental measurement.

[35] C. Liu, J. H. Mao, H. Ding, R. Wu, C. J. Tang, F. S. Li, K. He, W. Li, C. L. Song, X. C. Ma, Z. Liu, L. L. Wang, and Q. K. Xue, Phys. Rev. B **97**, 024502 (2018).
[36] H. M. Zhang, Z. Z. Ge, M. Weinert, and L. Li, Commun. Phys. **3**, 75 (2020).
[37] D. Huang, T. A. Webb, C. L. Song, C. Z. Chang, J. S. Moodera, E. Kaxiras, and J. E. Hoffman, Nano Lett. **16**, 4224 (2016).
[38] F. Li, Q. Zhang, C. Tang, C. Liu, J. Shi, C. Nie, G. Zhou, Z. Li, W. Zhang, C.-L. Song, K. He, S. Ji, S. Zhang, L. Gu, L. Wang, X.-C. Ma, and Q.-K. Xue, 2D Mater. **3**, 024002 (2016).
[39] S. O'Sullivan, R. Kang, J. A. Gardener, A. J. Akey, C. E. Matt, and J. E. Hoffman, Phys. Rev. B **105**, 165407 (2022).
[40] B. Sacépé, M. Feigel'man, and T. M. Klapwijk, Nat. Phys. **16**, 734 (2020).
[41] W. Li, H. Ding, P. Deng, K. Chang, C. Song, K. He, L. Wang, X. Ma, J.-P. Hu, X. Chen, and Q.-K. Xue, Nat. Phys. **8**, 126 (2012).
[42] B. Shen, B. Zeng, G. F. Chen, J. B. He, D. M. Wang, H. Yang, and H. H. Wen, Europhys. Lett. **96**, 37010 (2011).
[43] T. Berlijn, P. J. Hirschfeld, and W. Ku, Phys. Rev. Lett. **109**, 147003 (2012).
[44] J. C. Zhuang, W. K. Yeoh, X. Y. Cui, J. H. Kim, D. Q. Shi, Z. X. Shi, S. P. Ringer, X. L. Wang, and S. X. Dou, Appl. Phys. Lett. **104**, 262601 (2014).
[45] Y. Fang, D. H. Xie, W. Zhang, F. Chen, W. Feng, B. P. Xie, D. L. Feng, X. C. Lai, and S. Y. Tan, Phys. Rev. B **93**, 184503 (2016).
[46] M. Ren, Y. Yan, X. Niu, R. Tao, D. Hu, R. Peng, B. Xie, J. Zhao, T. Zhang, and D. L. Feng, Sci. Adv. **3**, e1603238 (2017).
[47] C. Liu, A. Kreisel, S. Zhong, Y. Li, B. M. Andersen, P. Hirschfeld, and J. Wang, Nano Lett. **22**, 3245 (2022).